Palaeogeography, Palaeoclimatology, Palaeoecology 512 (2018) 106–117

Contents lists available at ScienceDirect

Palaeogeography, Palaeoclimatology, Palaeoecology

journal homepage: www.elsevier.com/locate/palaeo

Global warming and rainfall: Lessons from an analysis of Mid-Miocene climate data

Zhengchuang Hui[a,*], Jun Zhang[a], Zhenhua Ma[a], Xiaomiao Li[a], Tingjiang Peng[a], Jijun Li[a], Bao Wang[b]

[a] Key Laboratory of Western China's Environmental Systems (Ministry of Education), College of Earth and Environmental Science, Lanzhou University, Lanzhou 730000, China
[b] School of Environmental & Municipal Engineering, Xi'an University of Architecture and Technology, Xi'an 710055, China

ARTICLE INFO

Keywords:
Sporopollen
Climatic gradient and seasonality
Northern Central China

ABSTRACT

The Mid-Miocene Climatic Optimum (MMCO) has been regarded as an analog for future global warming due to its scale of warming being equivalent to the warming predicted for the next century by the International Panel on Climate Change (IPCC)'s fourth report. However, little is known about how the MMCO influenced paleoprecipitation in central China. In this study, two pollen floras from the eastern Longzhong Basin, northern central China, were quantitatively analyzed to reconstruct the climatic conditions likely during the MMCO. The paleoclimatic parameters obtained by applying the Coexistence Approach (CoA) to these two palynological assemblages showed that the mean annual temperature (MAT, 16.6 °C) for the MMCO was 5.7 °C higher than the present-day MAT (10.9 °C), and that mean annual precipitation (MAP, 955.4 mm) was 413.5 mm higher than at present (541.9 mm), indicating a much warmer and wetter climate. The higher mean temperature for the coldest month (CMT) and the minimum monthly precipitation (MiMP) values also indicate a warmer and wetter coldest and driest month, respectively, and thus suggest the prevalence of a more balanced seasonal paleoclimate in northern central China. These climatic conditions are equivalent to higher global temperatures of ~5–6 °C during the MMCO. This finding would imply that precipitation in northern central China will increase in the context of ongoing global warming.

1. Introduction

The Mid-Miocene Climate Optimum (MMCO) occurred at ~17–15 Ma, and is one of the most recent global warming climatic events known to be unrelated to human activity during the period of stepwise Cenozoic cooling (Shackleton and Kennett, 1975; Zachos et al., 2001). Geological records indicate that mid-latitude temperatures were ~5–6 °C higher than at present during the MMCO (Flower and Kennett, 1994). This scale of warming is equivalent to the warming predicted for the next century by the IPCC's fourth report (IPCC (Intergovernmental Panel on Climate Change), 2007). The MMCO can therefore provide an analog for understanding future global warming. Recent research has focused on understanding the mechanisms driving the MMCO, as well as reconstructions of its paleotemperatures (You et al., 2009; You, 2010; Tong et al., 2009; Herold et al., 2011, 2012; Foster and Rohling, 2012; Miao et al., 2012; Goldner et al., 2014; Kochhann et al., 2016). A few studies have emphasized the significance of variations in precipitation within this warming period. East Asia is one of the most densely populated regions in the world; more than one fifth of the world's population lives in it. The maintenance of socioeconomically sustainable development in this populous region therefore depends critically on water delivery. As the delivery of water is critical to modern socioeconomic development, the study of any changes in precipitation during the MMCO may, in the context of ongoing global warming, be more applicable to the regions of East Asia (*e.g.*, the semi-humid regions of the Asian interior) where such increases and/or decreases in MMCO precipitation remain unknown. The MMCO in northern China was recorded in pollen assemblages (Hui et al., 2011, 2017; Miao et al., 2011), mammalian fossils (Deng, 2016), pedogenic iron oxides (Zhao et al., 2017), clay minerals (Song et al., 2017), lithology and rock magnetism (Zan et al., 2015), in lake geochemistry (Lebreton-Anberree et al., 2016) in southwestern China, and in continental chemical weathering and physical erosion (Wan et al., 2009) in the South China Sea. However, these records cannot provide direct information in the form of climatic parameters such as temperature and precipitation. In order to address this issue, it is necessary to conduct

* Corresponding author.
E-mail address: huizhch@lzu.edu.cn (Z. Hui).

https://doi.org/10.1016/j.palaeo.2018.10.025
Received 5 January 2018; Received in revised form 7 August 2018; Accepted 24 October 2018
Available online 31 October 2018
0031-0182/ © 2018 Elsevier B.V. All rights reserved.

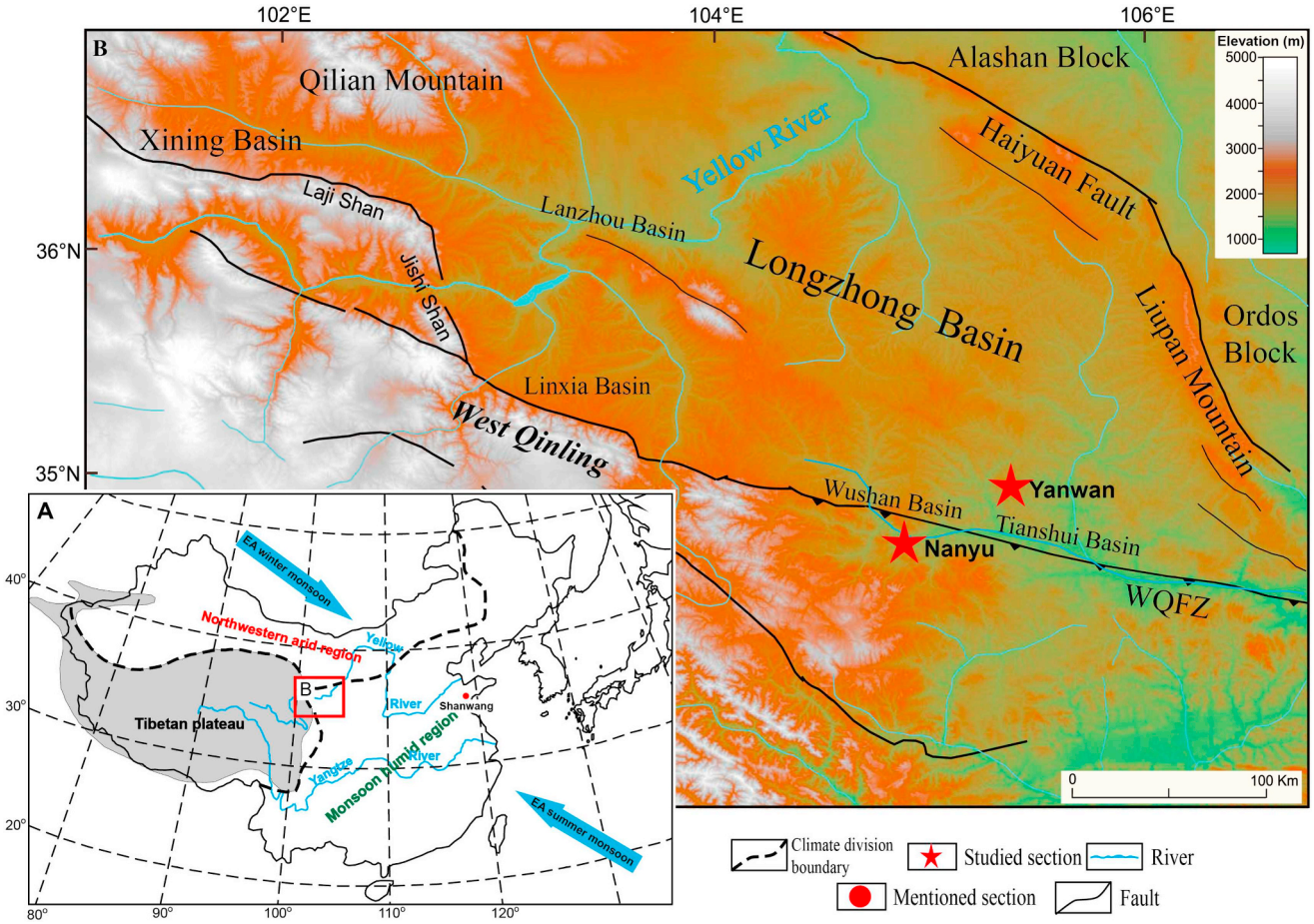

Fig. 1. Geological setting of study area, locations of the studied sections, and other locations mentioned in the text.

quantitative studies of climatically-sensitive proxy data obtained from long, continuous and well-dated Miocene sedimentary sequences. Along the northeastern margins of the Tibetan Plateau, the thick, continuous and mammal fossil-bearing Cenozoic deposits in the Longzhong Basin provide great potential for studying the paleoclimatic changes and tectonic history of the Miocene (Fig. 1A, B; Wang et al., 2012; Lease, 2014; Hou et al., 2015; Wang et al., 2016, 2017; Liu et al., 2016; Peng et al., 2016; Wu et al., 2017). In this study, we combined two previously-published pollen flora databases with a new pollen database obtained from the Tianshui Basin to reconstruct the MMCO's paleoclimatic history (Hui et al., 2011, 2017). In order to obtain the climatic parameters for the MMCO in this semi-humid region of the Asian interior, the Coexistence Approach (CoA; Mosbrugger and Utescher, 1997; Utescher et al., 2014) was applied to both the older and the newer pollen flora databases.

2. Geological and geographical setting

The Longzhong Basin, bounded by the Liupan Mountains to the east, the West Qinling Mountains to the south, the Laji-Qilian Mountains to the west and the Haiyuan Fault to the north (Fig. 1A, B), is located on the northeastern margins of the Tibetan Plateau, northern central China. Geographically, the Longzhong Basin sits at the conjunction of a humid monsoonal zone, the arid zone of northwest China, and the Tibetan Plateau, just at the apex of the so-called 'monsoon triangle' (Li et al., 1988; Fig. 1A), in a region highly sensitive to climate change. The Tianshui Basin and the Wushan Basin, two of the Longzhong Basin's sub-basins, are elongated Cenozoic basins that lie along the West Qinling Fault Zone (WQFZ) in the eastern part of the Longzhong Basin (Fig. 1B). The Cenozoic successions distributed in the Longzhong Basin (including these two subbasins) were originally divided into the Paleogene "Guyuan Group" and the Neogene "Gansu Group" according to lithofacies and paleontology (Zhai and Cai, 1984). The Paleogene sediments, which mostly consist of massive purple-reddish, grey-white conglomerates and sandstones and abundant coarse breccia with thicknesses varying between several tens to hundreds of meters, are exposed only at a few places within the Tianshui and Wushan Basin (Zhai and Cai, 1984; Zhang et al., 2013; Supplementary Fig. S1). These Paleogene sediments are uncomfortable with the overlying Neogene sediments and the underlying older metamorphic rocks (Li et al., 2006). In contrast to Paleogene sediments, Neogene sediments are widely exposed within the Tianshui Basin and Wushan Basin and most of the exposed Neogene sediments within these basins are covered by Quaternary loess (Supplementary Fig. S1). The widely-distributed, continuous and well-dated mudflat/distal fans, floodplains and shallow lake Neogene deposits in these sub-basins provide a suitable resource for the investigation of the MMCO in this semi-humid region of the Asian interior (Zhang et al., 2013; Liu et al., 2015; He, 2013). The studied sections, named Yanwan and Nanyu, are located in the Tianshui Basin and the Wushan Basin, respectively (Fig. 1B; Hui et al., 2011, 2017). According to previous work, the Neogene strata in the Yanwan section can be divided into three units from bottom to up: Unit 1 (132 m) consists mainly of fine-grained light brown-yellow mudstones intercalated with brown-red mudstones, including argillaceous siltstones with horizontal bedding, sandstone lenses, and brick-red poorly sorted conglomerate at the base; Unit 2 (128 m) consists mainly of light blown-yellow calciferous mudstones interbedded with browned mudstones with fine laminations; Unit 3 (28 m) consists of brown-red and brown-yellow mudstones with horizontal bedding and grey-green bands (Alonso-Zarza et al., 2009; Zhang et al., 2013). In the Nanyu

section, at depths of 0–80 m and 127–158 m, the lithology is principally composed of grey-green marlstone, brown-red mudstone and brown siltstone, with occasional grey-green sandstone. The grey-green marlstone and brown siltstone contain horizontal beddings. At the 80–127 m and 158–244 m depths in this section, the lithology consist of siltstone with calcareous nodules, mudstone and fine sandstone lenses (He, 2013; Liu et al., 2015). Previous paleomagnetic and biostratigraphic work has indicated that the Yanwan and Nanyu Sections were formed between 6.1 and 17.1 Ma and 13.6–16.1 Ma, respectively (Zhang et al., 2013; Liu et al., 2015; Supplementary Fig. S1). In this study, we focused on the MMCO period during Yanwan (288–225 m depth, 14.6–17.1 Ma) and Nanyu section being deposited (153–244 m depth, 15–16.1 Ma; see Supplementary Fig. S1).

At present, the climate in this region is dominated by the East Asian Monsoon (EAM), and is therefore characterized by hot-humid summers and cold-dry winters. According to data in the *Land Climate of China* (1971–2000) (IDBMC (Information Department of Beijing Meteorological Center), 2005), the MAT is ~10 °C, with a July monthly mean of 24.8 °C, and a January monthly mean of −2 °C. MAP is 491.6 mm, with most annual precipitation falling during the July to September period.

3. Materials and methods

67 MMCO sedimentary samples were collected from the Yanwan Section in the Tianshui Basin for pollen analysis; 12 of these have been previously reported upon by Hui et al. (2011). The 60 MMCO pollen data from the Nanyu Section in the Wushan Basin were reported upon by Hui et al. (2017). In the laboratory, the samples were processed following conventional palynological procedures (Fagri and Iversen, 1989), including treatment with 10% HCl and 39 HF to remove carbonates and silica, and heavy liquid ($ZnCl_2$) to concentrate the pollen grains. Finally, all the processed samples were stored in 10 ml plastic test tubes for identification. All pollen samples were identified at the College of Earth and Environment Sciences, Lanzhou University. Pollen identification was conducted under an Olympus light microscope, with the help of officially-published modern and fossil pollen atlases (Wang et al., 1995; Song, 1999). Pollen diagrams were prepared using Tilia software (Grimm, 1993).

In order to obtain climatic parameters, the CoA, developed by Mosbrugger and Utescher (1997), was applied to the MMCO Yanwan and Nanyu sections' palynological flora data. Following the procedure used to obtain the climatic tolerance (Mosbrugger and Utescher, 1997; Kou et al., 2006; Utescher et al., 2014), seven climatic parameters were delineated, *i.e.*, the MAT, the mean temperature of the warmest month (WMT), the mean temperature of the coldest month (CMT), MAP, the maximum monthly precipitation (MaMP), and the minimum monthly precipitation (MiMP) (Table 3).

4. Pollen records

In the Yanwan Section, only 27 (including the 12 samples from Hui et al.'s (2011) paper) of the 67 sedimentary samples contained > 100 sporopollen grains. The other 60 samples from the Nanyu Section (taken from Hui et al. (2017)), were rezoned for this study. A total of 90 different palynomorphs were identified in the Yanwan and Nanyu sections at the *genus* or family level (Supplementary Table S1). The arboreal pollen taxa included mainly *Pinus*, *Cedrus*, *Podocarpus*, *Picea*, *Abies*, *Taxodiaceae*, *Cupressaceae*, *Betula*, *Quercus*, *Ulmus*, *Juglans*, *Rhus*, *Salix* and *Fraxinus*. The pollen of subtropical plants such as *Liquidambar*, *Pterocarya*, *Carya* and *Castanea* were also observed in some samples. The scrubby and herbaceous taxa identified were mostly *Elaeagnaceae*, *Celastraceae*, *Poaceae*, *Artemisia*, *Chenopodiaceae*, *Ranunculaceae* and *Rosaceae*. The aquatic plants *Typhaceae*, *Cyperaceae* and *Potamogeton* occurred only in some samples, and then with very low abundances. A few pteridophyte spores were also identified, *e.g. Polypodiaceae*, *Pteridaceae* and *Polypodium*. Based on variations in the relative abundance of important and common taxa and the relative proportions of trees, shrubs and herbs, the Yanwan and Nanyu pollen assemblages were divided into three and two pollen zones, respectively (Figs. 2, 3).

4.1. Yanwan Section pollen assemblages

Zone 1 (*depth*: *288–271 m*; *age*: *17.1–16.2 Ma*; *11 samples*) is characterized by a relatively high abundance of shrubby and herbaceous pollens (37.3%–59.1%), mainly from *Ranunculaceae* (3.4%–19.5%), *Artemisia* (6.3%–21.7%), *Chenopodiaceae* (2%–16.2%) and *Elaeagnaceae* (0–9.3%). The abundance of arboreal pollens (39.4%–62.3%) is slightly lower than that of shrubby and herbaceous pollens, with *Betula* (1.4%–6.7%), *Quercus* (2.3%–5.9%), *Ulmus* (5.4%–15.2%), *Fraxinus* (0–6.9%) and *Salix* (6.2%–16.2%) being commonly-observed types. Subtropical broadleaved arboreal pollens, such as *Liquidambar*, *Pterocarya*, *Sapindaceae* and *Carya* are also observed in very low abundances, but occur consistently throughout the whole section. Aquatic plant pollens, such as *Cyperaceae*, *Typhaceae* and *Potamogeton*, and fern spores, occur in only a few samples during this section's studied period and even then at very low percentages (Fig. 2, Table 1).

Zone 2 (*depth*: *271–258.25 m*; *age*: *16.2–15.8 Ma*; *six samples*) shows a marked increase in *Betula* (4.5%–35.5%), *Quercus* (3.7%–14.4%), *Rhus* (0–5.9%) and *Pinus* (0–8.6%) pollens, leading to a significant increase in the overall proportion of arboreal pollens (53%–66.4%); conversely, the broadleaved taxa *Ulmus* (0.7%–4.3%) and *Salix* (2.7%–22.3%) decrease markedly. Shrubby and herbaceous pollen percentages (20%–47%) decline, mainly due to a decrease in Chenopodiaceae (1%–5%), Ranunculaceae (2.4%–14.1%) and *Artemisia* (0–11.1%), whereas mesophytic taxa, *e.g.* Poaceae (2.2%–12.5%), exhibit a clear increase (Fig. 2, Table 1).

Zone 3 (*depth*: *258.25–225.25 m*; *age*: *15.8–14.6 Ma*; *10 samples*) shows a decrease in arboreal pollen percentages (46%–79.2%), resulting principally from the decrease in *Betula* (1%–33.5%) and *Quercus* (0–15.6%) pollens, although *Salix* (2.8%–22.3%) and *Ulmus* (0.7%–23.7%) taxa display a clear increase. Shrubby and herbaceous pollen percentages (20.8%–48.5%) increase slightly, mainly due to an increase in *Artemisia* (0–10.8%), *Poaceae* (0–12.1%), *Elaeagnaceae* (0–11.3%) and *Ranunculaceae* (5.1%–10.8%) pollen percentages (Fig. 2, Table 1).

4.2. Nanyu Section pollen assemblages

Zone 1 (*depth*: *244–182 m*; *age*: *16.1–15.4 Ma*; *32 samples*) is characterized by high arboreal pollen percentages (47.5%–82.7%) and a slight decrease in arboreal pollen percentages. Based on the variations in *Cupressaceae*, *Cedrus*, *Betula*, *Ulmus* and *Poaceae* pollen percentages, this zone can be further divided into two subzones, thus (Fig. 3, Table 2):

Subzone 1a (*depth*: *244–198 m*; *age*: *16.1–15.6 Ma*; *21 samples*). In this subzone, the outstanding feature is the peak in *Cedrus* pollen percentages (1.9%–60.8%), although its proportion fluctuates sharply and gradually decreases. Cupressaceae (0–12.2%) and *Pinus* (0–7%) are observed in small percentages. *Betula* (0.7%–24.8%), *Ulmus* (1.5%–16.8%), *Salix* (0.8%–34%) and *Quercus* (0–10.1%) are the most important and common broadleaved trees represented, but there are also small subtropical elements, such as *Castanea*, *Pterocarya* and *Carya*. Shrubby and herbaceous taxa mainly consist of Elaeagnaceae (0–8.7%), *Artemisia* (6.3%–29.8%) and Chenopodiaceae (0.8%–12.4%), accompanied by *Poaceae*, *Cruciferae* and *Ranunculaceae*. Aquatic plant pollens, such as *Potamogeton* and *Typhaceae*, are also observed in some samples, although their abundances are very low.

Subzone 1b (*depth*: *198–182 m*; *age*: *15.6–15.4 Ma*; *11 samples*). This subzone is marked by a sharp decrease in *Cedrus* pollen percentages (1.5%–8.6%), resulting in a slight overall reduction in the total arboreal pollen percentage (47.5%–82.7%). Broadleaved taxa, mainly consisting

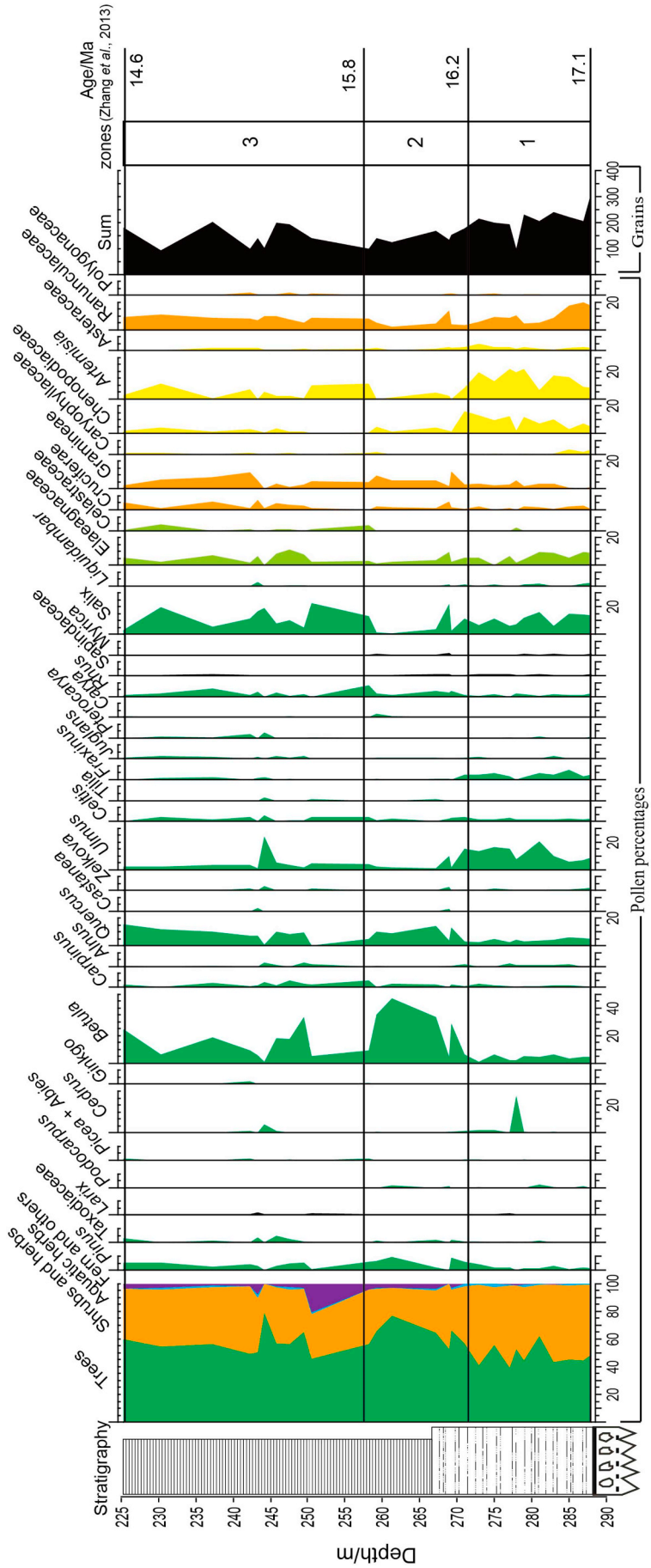

Fig. 2. Pollen diagram and lithology of the Yanwan Section in the Tianshui Basin (part of pollen data from Hui et al., 2011).

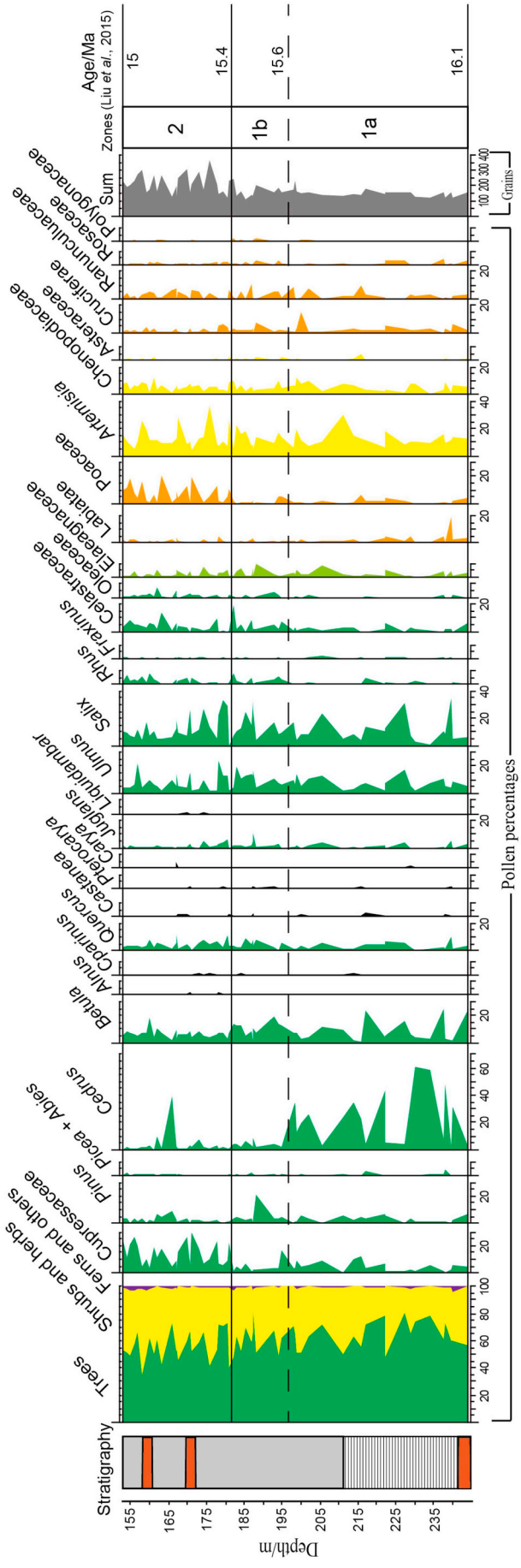

Fig. 3. Pollen diagram and lithology of the Nanyu Section in the Wushan Basin (Hui et al., 2017).

Table 1
List of the Middle Miocene Yanwan section palynomorph taxa grouped by ecological requirements and their relative abundance in the three zones.

Zone	1 (%)	2 (%)	3 (%)	Zone	1 (%)	2 (%)	3 (%)
Megathermic elements				*Larix*	0.3	/	0.3
Sapindaceae	0.3	0.2	0.1	*Abies*	0.1	0.2	0.1
Rutaceae	/	/	0.1	*Picea*	0.2	/	0.3
Mega-mesothermic elements				Non-significant elements			
Liquidambar	0.7	0.1	0.4	*Rosaceae*	0.7	1.5	1.5
Hamamelidaceae	0.2	/	/	Herbs & shrubs			
Celastraceae	0.2	0.7	0.9	*Berberidaceae*	0.1	0.1	/
Euphorbiaceae	/	/	0.1	*Gentianaceae*	/	/	0.1
Cedrus	3	0.4	0.8	*Leguminosae*	0.3	0.5	0.5
Myrica	0.1	0.2	/	*Caryophyllaceae*	0.9	0.4	0.5
Taxodiaceae	0.4	0.9	1.7	*Verbenaceae*	0.2	/	0.2
Mesothermic elements				Labiate	0.3	/	0.4
Ginkgo	0.1	0.2	0.2	*Polygnoaceae*	0.3	0.5	0.6
Ulmus	11.8	3.3	4.9	*Cruciferae*	1.3	2.1	3.4
Zelkova	0.6	0.4	0.5	*Rubiaceae*	/	/	0.1
Celtis	1.5	1.6	1.5	*Umbelliferae*	/	/	0.1
Quercus	4.1	9.2	8.1	*Amaranthaceae*	/	0.2	/
Castanea	0.1	0.2	0.2	*Vitaceae*	/	0.4	/
Ostryopsis	/	/	0.1	*Ranunculaceae*	10	6.4	8.4
Betula	4.4	26.5	14	*Chenopodiaceae*	8.9	2.5	2
Alnus	0.9	0.4	0.9	*Artemisia*	14.4	3.2	4.1
Carpinus	1	1.9	2.3	*Poaceae*	2.9	7	5
Pteroceltis	/	/	0.2	*Asteraceae*	2.2	1.4	1.1
Eupteleaceae	0.1	/	0.3	*Nitraria*	1	0.7	0.5
Juglans	0.6	0.4	1.1	*Ephedra*	0.1	/	0.1
Carya	0.1	0.6	0.2	*Typha*	0.1	0.1	0.1
Pterocarya	0.2	/	0.9	*Cyperaceae*	0.9	0.1	0.3
Populus	0.5	0.2	0.6	*Potamogeton*	0.1	0.2	0.2
Rhus	1.2	3.5	1.9	*Myriophyllum*	/	/	0.2
Tilia	/	0.1	0.3	*Urticaceae*	0.3	0.7	1.1
Oleaceae	/	0.1	0.1	*Papaveraceae*	/	/	0.1
Fraxinus	3.3	0.3	0.6	*Plantagiaceae*	/	/	0.4
Fagus	0.1	/	/	*Thalictrum*	/	/	0.1
Salix	10.8	7.2	11.9	*Acanthaceae*	0.1	/	1
Buxus	0.1	/	/	*Caprifoliaceae*	0.1	/	/
Podocarpus	0.3	0.4	/	*Pteridophytes*			
Elaeagnaceae	6	3.8	5.2	*Lycopodium*	/	/	0.1
Simaroubaceae	/	0.2	/	Other elements			
Meso-microthermic elements				*Qinghaipollis*	/	0.2	/
Pinus	2	5.4	3.3	*Triletes*	/	/	0.3
Tsuga	/	0.1	/	*Tricolpopollenites*	/	0.1	0.2
Microthermic elements				Unidentified	0.2	2.6	4.1

of *Betula* (0.8%–19%), *Quercus* (0–9%), *Ulmus* (3.8%–18.9%) and *Salix* (3.6%–32.3%), appear relatively stable. Shrubby and herbaceous pollen percentages, *i.e.*, of *Artemisia* (3.6%–22%), *Poaceae* (0–5.6%) and *Chenopodiaceae* (2.2%–10.1%), exhibit no obvious change compared with those of Subzone 1a. The aquatic plant pollens *Potamogeton* and Typhaceae, as well as some fern spores (*e.g.*, *Polypodiaceae*) are also present in some samples, but their abundances are very low.

Zone 2 (*depth*: *182–153 m*; *age*: *15.4–15 Ma*; *26 samples*) exhibits a continuous decrease in arboreal pollen percentages (34.6%–73.4%), resulting principally from the further decrease in *Cedrus* (0–39.1%) and *Betula* (1.6%–18.3%) pollen percentages, although there is also a notable increase in *Cupressaceae* pollen percentages (1.6%–30%). Broadleaved taxa, *i.e.*, *Quercus*, *Ulmus* and *Salix*, appear relatively stable. Herbaceous *Poaceae* pollen percentages (0.6%–20.7%) increase markedly, resulting in a clear increase in shrubby and herbaceous pollen percentages (24.2%–63.4%), dominated by *Artemisia* (3.8%–36.7%), *Chenopodiaceae* (1.6%–12.6%) and *Ranunculaceae* (0–7.2%; Fig. 3, Table 2).

5. Discussion

5.1. Paleovegetation

The two pollen assemblages from the Tianshui Basin and Wushan Basin suggest that, during the MMCO, the eastern Longzhong Basin was occupied by mixed coniferous and deciduous broadleaved forests growing under warm and humid climatic conditions. The co-occurrence of megathermic, megathermic-mesothermic and microthermic elements would indicate the existence of vertical vegetation zones covering the south-facing hillsides of the Longzhong Basin, and of broadleaved, deciduous, warm-temperate (principally *Betula*, *Quercus*, *Ulmus* and *Juglans*) and subtropical (*i.e.*, mainly *Liquidambar*, *Sapindaceae* and *Carya*) trees in the Basin's lowlands. *Salix*, *Alnus*, *Fraxinus* and *Taxodiaceae* appear to have been distributed along river banks or lake margins, with *Cyperaceae*, *Typhaceae* and *Myriophyllum* present along lake shores or in shallow water areas. Shrubs and herbs, principally *Celastraceae*, *Ranunculaceae*, *Poaceae*, *Chenopodiaceae* and *Artemisia*, covered the forest understory (Wu et al., 1980; Tables 1, 2; Figs. 1B, 4). Based on the three palynological zones described as existing within the Yanwan and Nanyu pollen assemblages, the Mid-Miocene vegetation succession in the eastern Longzhong Basin can be subdivided into three corresponding periods as follows (Fig. 4):

Period 1 (corresponding to Zone 1 in the Yanwan pollen assemblage, ~17–16 Ma): The abundances of shrubby and herbaceous pollens are almost equal to those of arboreal pollens. This would imply that the regional vegetation was probably composed of open, broadleaved deciduous forests (Xu et al., 2006), indicating a degree of woodland shrinkage and thus relatively drier climatic conditions compared with the other two periods.

Period 2 (corresponding to Zone 2 in the Yanwan pollen assemblage

Table 2
List of the Middle Miocene Nanyu section palynomorph taxa grouped by ecological requirements and their relative abundance in the three zones.

Zone	1a (%)	1b (%)	2 (%)	Zone	1a (%)	1b (%)	2 (%)
Mega-mesothermic elements				*Abies*	/	0.1	0.1
Liquidambar	/	/	0.1	Non-significant elements			
Celastraceae	1.7	4.8	3.5	*Rosaceae*	0.7	0.9	0.8
Cedrus	24.4	3.7	3.2	Herbs & shrubs			
Mesothermic elements				*Thalictrum*	/	0.1	/
Cupressaceae	4.5	4.2	13.9	*Humulus*	/	0.1	/
Podocarpaceae	/	/	0.1	*Caryophyllaceae*	/	/	0.1
Ulmus	7.1	10.8	7.6	*Polygnoaceae*	0.3	0.7	0.3
Celtis	0.1	/	/	*Verbenaceae*	/	/	0.1
Quercus	3	4.4	4.3	*Cruciferae*	2.8	2.3	1.9
Castanea	0.2	0.1	0.2	*Umbelliferae*	0.1	0.2	0.1
Betula	7.9	10.6	6.7	*Urticaceae*	0.1	/	/
Alnus	0.2	0.2	0.2	*Scrophulariaceae*	/	0.1	0.1
Carpinus	0.1	0.1	0.1	*Nitraria*	0.6	0.4	0.3
Ostryposis	/	/	0.1	*Ranunculaceae*	2.3	2.6	2.6
Rhamnaceae	/	/	0.1	*Chenopodiaceae*	5.6	5.1	5.9
Juglans	1.1	2.5	1.4	*Leguminosae*	0.1	0.1	/
Carya	0.1	/	0.2	*Artemisia*	12.4	12.2	13.3
Pterocarya	0.1	0.2	0.1	*Poaceae*	1.4	1.5	7.3
Thymelaeaceae	0.1	/	0.1	*Asteraceae*	0.6	0.8	0.6
Rhus	0.9	2.9	2.3	*Ephedra*	0.4	0.3	0.4
Tilia	0.1	/	/	*Typha*	0.1	0.6	0.3
Oleaceae	0.3	0.9	1.5	*Cyperaceae*	0.1	0.2	0.2
Fraxinus	0.3	0.3	0.3	*Potamogeton*	0.1	0.2	0.1
Salix	11.1	15.2	12.4	*Berberidaceae*	/	/	0.1
Ilex	/	/	0.1	*Solanaceae*	0.1	0.1	/
Elaeagnlaceae	2.4	3.1	2.3	*Caprifoliaceae*	/	/	0.1
Meso-microthermic elements				*Pteridophytes*			
Pinus	2.8	4.9	2.5	*Polypodiaceae*	0.1	0.2	0.1
Tsuga	/	/	0.1	Other elements			
Microthermic elements				*Triletes*	0.1	0.1	0.1
Picea	0.5	0.5	0.5	Unidentified	0.6	0.9	1

and Zone 1 in the Nanyu pollen assemblage, ~16–15.6 Ma): During this period, both pollen assemblages' arboreal pollen contents peaked, principally as a result of a dramatic increase in the pollen percentages of the cold-tolerant *Betula* and the cool-wet loving *Quercus* in the Yanwan Section, and the presence of significant quantities of humid-loving coniferous *Cedrus* pollens in the Nanyu Section, suggesting the existence of a cooler and more humid climate than during the other two periods.

Period 3 (corresponding to Zone 3 in the Yanwan pollen assemblage and Zone 2 in the Nanyu pollen assemblage, ~15.6–14.6 Ma): The decrease in percentages of *Betula* and *Quercus* pollens in the Yanwan section, and in percentages of *Cedrus* pollens in the Nanyu Section would suggest drying climatic conditions during this period, although still wetter than Period 1.

5.2. Paleoclimate

The MMCO climatic parameters of the Yanwan and Nanyu sections were estimated by applying the CoA method (Mosbrugger and Utescher, 1997), using palynological flora data. Supplementary Figs. S2 and S3 illustrate the full ranges in the values of these climatic variables, based on the 70 and 54 nearest living relatives (NLRs) of palynomorphs from the Yanwan and Nanyu pollen assemblages, respectively (Tables 1 and 2). For the Yanwan Section, the MAT = 14.2–18.9 °C, WMT = 22.5–26.6 °C, CMT = 2.5–7.8 °C, MAP = 797.5–1113.3 mm, MaMP = 241–264 mm and MiMP = 8.0–14.1 mm. All the Yanwan climatic parameters (except for the MaMP values) are either the same, or similar, to those observed for the Nanyu Section (Table 3), suggesting that climatic conditions in the eastern Longzhong Basin were roughly homogeneous during this period. When the Yanwan pollen assemblage is compared with Nanyu's, however, their main pollen taxa are distinctly different. It would therefore appear difficult to reconcile the differences in the predominant taxa between the two sections with the similar climatic parameters obtained from analyses of their respective NLRs. However, if the highland taxa (*e.g.*, those of coniferous *Cedrus* and Cupressaceae, which are today found in the southern Qinling Mountains closer to the Nanyu Section than to the Yanwan Section (Fig. 1B)) are removed from the Nanyu pollen assemblage, the other components (*i.e.*, lowland plants) in these two pollen assemblages appear very similar. The climatic conditions prevalent in inland basins are known to be principally reflected by the regional vegetation cover found distributed in their piedmonts (Wu et al., 1980). Any climatic parameters delineated by the coexistence tolerance of a basin's lowland plants would therefore reflect the climate of that basin, rather than that of the highlands or mountains surrounding it. Such an explanation would fully justify the similar climatic parameters obtained for the two different pollen assemblages at Yanwan and Nanyu.

5.3. Northern Chinese climatic seasonality and precipitation gradients during the MMCO

Although parts of Asia were flooded by the sea, the present shape of the Asian continent already existed during the Miocene (Scotese, 2002). The paleocoordinates of the study region have therefore not changed significantly since then. For this reason the meteorological data from a similar and/or the nearest geographical region can reasonably be used to compare today's climatic conditions with those of the Miocene in an attempt to explore the possible laws of climate change in the context of ongoing global warming. In this study, recent climate data from the Tianshui meteorological station (located 45 km southeast of the Yanwan Section and 70 km east of the Nanyu Section, in the Tianshui Basin; Fig. 1B) was chosen to represent the recent climatic conditions of the eastern Longzhong Basin and was therefore used in our comparisons with the climatic conditions prevalent during the Miocene. The climate data from the Tianshui meteorological station describe a highly typical monsoonal climate model: the principal rainy season occurs between

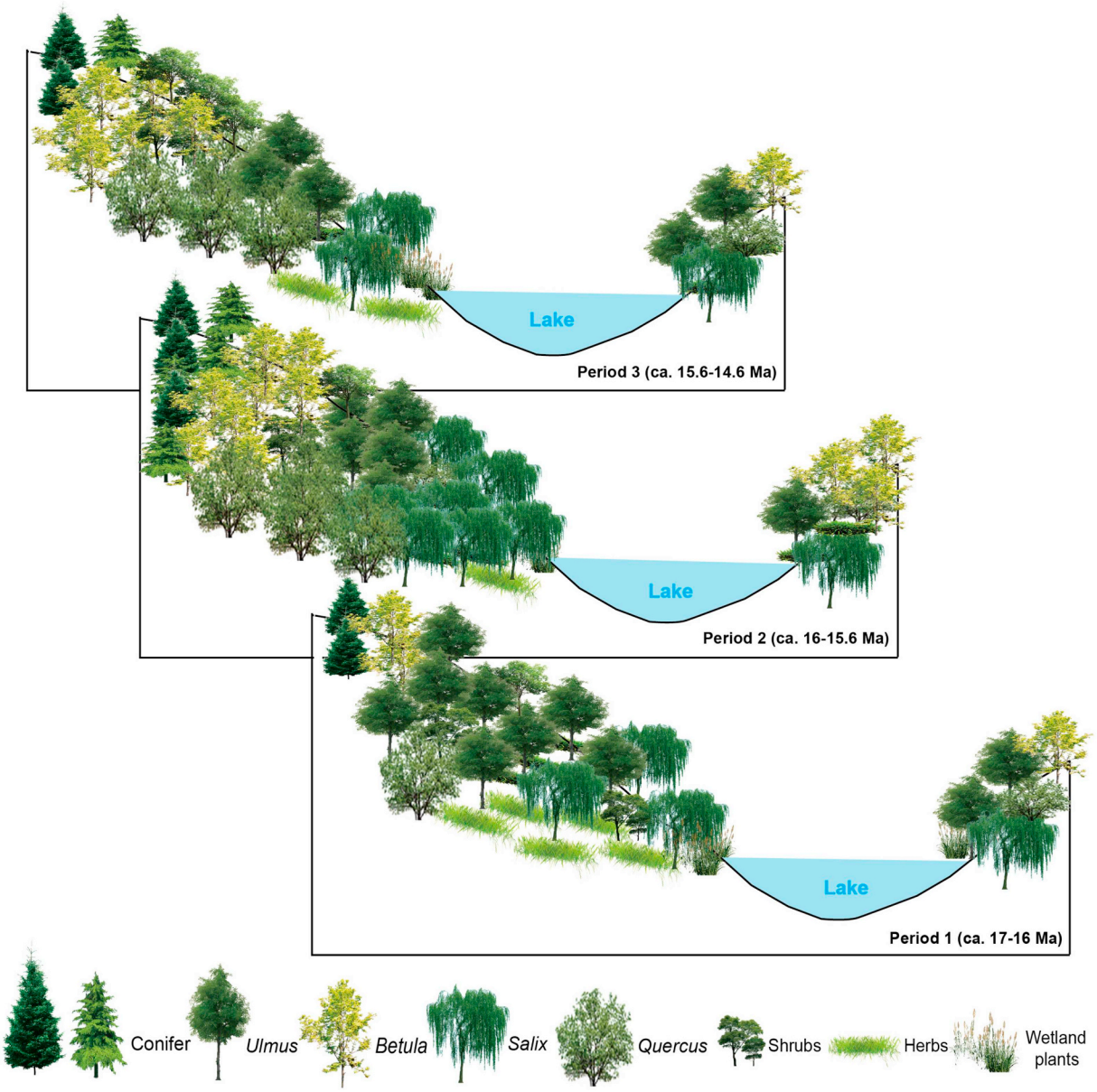

Fig. 4. Reconstruction of vegetation successions based on a MMCO pollen diagram of the eastern Longzhong Basin (Figs. 2, 3).

June and September (*e.g.*, the East Asian summer Monsoon (EASM)), and the least precipitation falls during the winter months (December–February) (Fig. 5A). March to May (Spring) and October to November (Autumn) represent the transitions between the seasons.

The reconstructed paleoclimatic parameters for the Yanwan and Nanyu pollen flora document a seasonal precipitation pattern with a dry and a wet period, with much higher precipitation during the warmest period. This seasonality is similar to that of the recent annual precipitation cycle in observed in the Tianshui Basin and seems to prove the presence of a monsoon-like atmospheric circulation over northern

Table 3
The climatic parameters of MMCO in eastern Longzhong, Shanwang Basin and recent climate data record of Tianshui and Weifang, northern China.

Climatic parameters		Middle Miocene		Modern	
MAT (°C)	18.9–14.2[a]	18.9–14.2[b]	17.2–15.3[c]	10.9[d]	12.9[e]
WMT (°C)	26.6–22.5[a]	26.6–22.5[b]	27.8–24.7[c]	28.5–17.9[d]	30.9–21.8[e]
CMT (°C)	7.8–2.5[a]	11.9–1.9[b]	7–5[c]	3.1-(−6.4)[d]	2.8-(−7.6)[e]
MAP (mm)	1113.3–797.5[a]	1113.3–797.5[b]	1281–996[c]	541.9 [d]	631.7[e]
MaMP (mm)	264–241[a]	268.1–141.5[b]	–	93 [d]	181.4[e]
MiMP (mm)	14.1–8[a]	14.1–6.9[b]	–	3.3 [d]	7.8[e]

[a, b] and [c] are Middle Miocene climatic parameters reconstructed based on Yanwan, Nanyu (this study) and Shanwang (Liang et al., 2003) pollen assemblage, respectively.
[d] and [e] are the recent climate data record of Tianshui and Weifang from (IDBMC (Information Department of Beijing Meteorological Center), 2005) (data from 1971 to 2000) and World Climate database (http://www.worldclimate.com/).

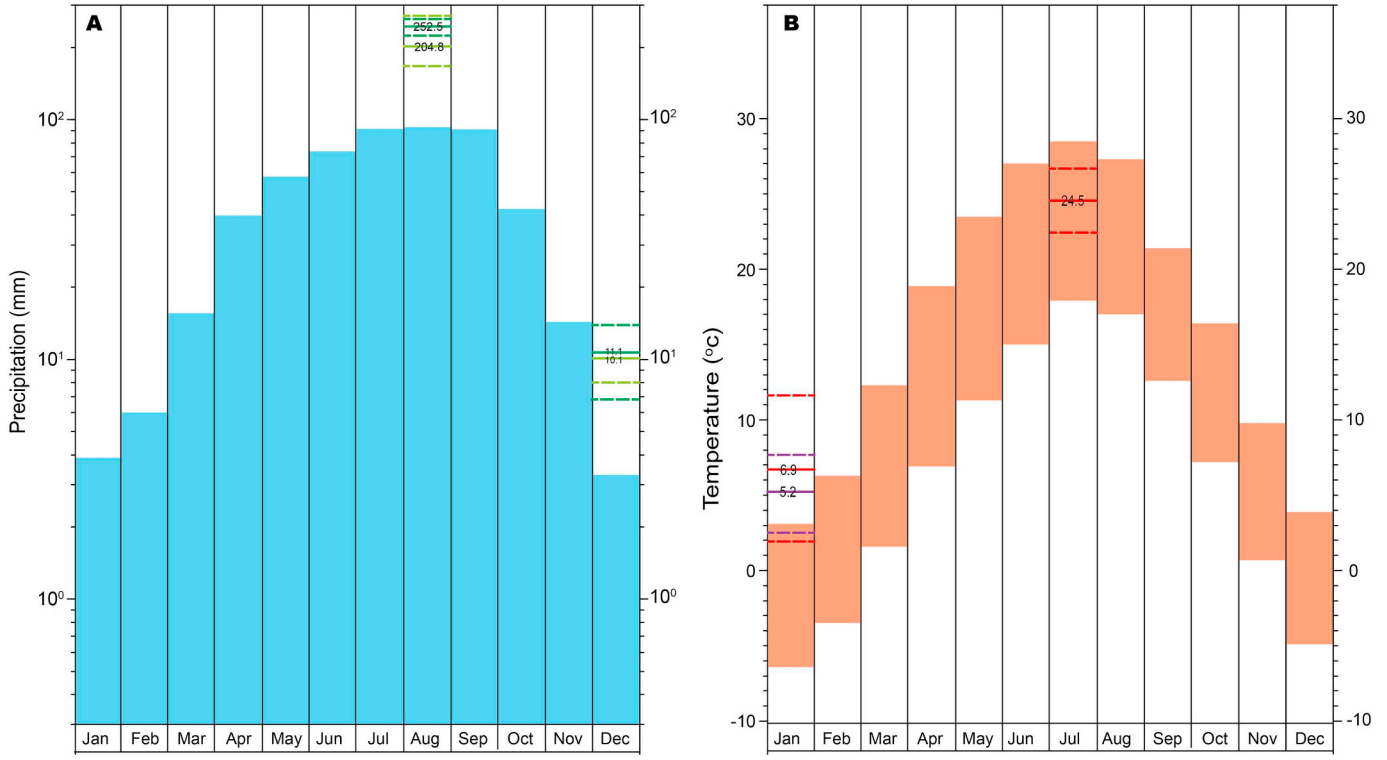

Fig. 5. Recent annual climate cycle in the Tianshui Basin. Recent precipitation and temperature data were compiled using the Worldclimate database (http://www.worldclimate.com; mean monthly temperature = brown columns; mean monthly precipitation = blue columns). The dashed red, pink (temperature) and green, light green (precipitation) lines show the coexistence intervals of the Yanwan and Nanyu flora assemblages' climatic parameters, respectively; the solid lines indicate the corresponding mean values. (For interpretation of the references to colour in this figure legend, the reader is referred to the web version of this article.)

China during the MMCO. The mean MAP value for the Miocene is almost twice the present MAP at Tianshui (Table 3). The mean values of the coexistence intervals for the Miocene MiMPs and MaMPs indicate a slightly more balanced rainfall pattern, with, respectively, a wetter driest and coldest month, and a wetter warmest and wettest month compared to today (Fig. 5A and B). Because the rainfall seasonality weakens towards the southeast in East Asia today (the distance to China's southeastern coast is the critical constraint for the strength of seasonal rainfall), a closer relative distance between our study region and the southeast Asian coast may have been responsible for this slightly more balanced rainfall seasonality (Wang, 1999; Scotese, 2002). The mean values of the MAT and CMT coexistence intervals for the Miocene are higher than for the present day, whereas the WMT is lower (Table 3, Fig. 5B). The higher Miocene CMTs and lower Miocene WMTs account for the differences between Miocene and recent datasets, pointing to a lower temperature seasonality, warmer winters and cooler summers during the Miocene than today.

Up until now, the Shanwang Basin (Figs. 1A, 7) is the only studied region in northern China which has had its MMCO climatic parameters quantitatively delineated (with an absolute age control of 17–15.2 Ma) (Sun et al., 2002; Liang et al., 2003; Yang et al., 2007). The Shanwang Basin, Tianshui Basin and Wushan Basin not only have similar latitudes (Fig. 1A), but are also distributed in modern China's semi-humid region (Atlas of Physical Geography in China, 2000). Their MMCO climatic parameters can therefore be compared when exploring the Miocene precipitation gradient in northern China. When comparing temperature parameters, the MAT, WMT and CMT mean coexistence intervals are very similar (Table 3, Fig. 6B). This similarity may be a result of the similar latitudes and thus climatic zones in which these basins are located, if one assumes that they all receive similar quantities of solar radiation. However, as a general rule, the Shanwang Basin's rainfall parameters show a more balanced rainfall pattern than those of the eastern Longzhong Basin (Table 3). Indeed, the Miocene MAP mean coexistence interval for the eastern Longzhong Basin is 17% lower than the Miocene MAP for the Shanwang Basin. This can be explained by the Shanwang Basin's location in the eastern part of China close to the ocean (a water source). Recent climate data show that the modern MAP at Tianshui (eastern Longzhong Basin) is 15% lower than the Shanwang Basin's MAP (the latter values being derived from climate data for Weifang City), indicating that any difference in the MAP gradient between the Miocene and today is insignificant (Table 3, Fig. 6A). The Miocene MAP values for the eastern Longzhong Basin and the Shanwang Basin would also indicate that these basins were located in a humid region during the MMCO, implying that such a humid region expanded towards the northwestern part of China during the MMCO and was therefore more extensive than it is today. Based on the spatial and temporal variations in percentages of *Fupingopollenites* (an extinct palynomorph) distributed across Inner and East Asia, Miao et al. (2016) found that the latter humid region reached at least as far as the eastern Qaidam Basin (~36°N, 97.5°E) during the Mid-Miocene (~17–11 Ma), and that the MAP in eastern China (approximately south of 40°N, and east of 90°E) was > 1000 mm. Our results are consistent with these findings, although the mean Miocene MAP for the eastern Longzhong Basin is slightly < 1000 mm.

In summary, the reconstructed Mid-Miocene climatic parameters based on palynological floras suggest that wetter, warmer and more balanced climatic conditions prevailed in northern and eastern China during this time, and that the spatial differences between the precipitation gradients of eastern and central China were similar to those of today.

5.4. Influence of Miocene global warming and the uplift of the Tibetan Plateau on the northern Chinese climate

The CoA values for the Yanwan and Nanyu pollen flora databases indicate the existence of a wetter, warmer and more seasonally-

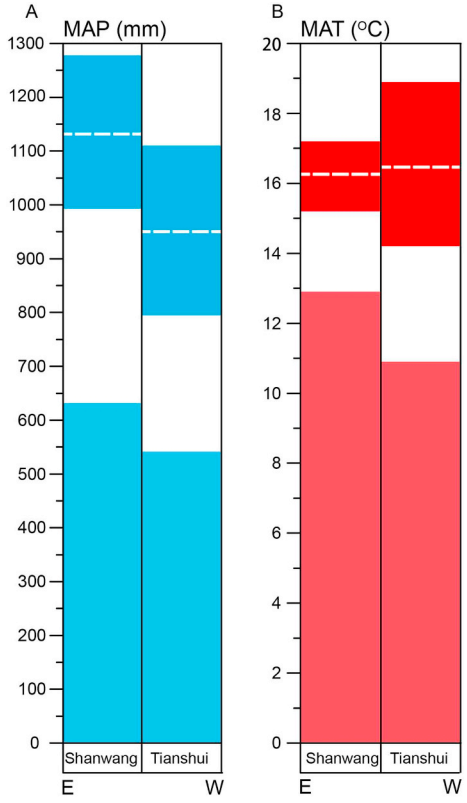

Fig. 6. West-east gradient of MAP and MAT in northeastern China. A and B are the MAP and MAT, respectively. Recent climate data (light blue and red) were taken from the Worldclimate database (http://www.worldclimate.com). Blue and red are the coexistence intervals for the MMCO MAP and MAT (dashed white bars are the mean values), respectively. (For interpretation of the references to colour in this figure legend, the reader is referred to the web version of this article.)

balanced paleoclimate during the MMCO. According to the Flower and Kennett (1994), MMCO temperatures were ~6 °C higher in the mid-latitudes than they are today. Climate simulations have suggested that the global annual mean surface temperature was 18.4 °C during the MMCO, ~3 °C higher than it is today (You et al., 2009). Our studies indicate that the mean MMCO MAT was ~ 5.5 °C higher than it is today (Table 3), a finding which is very similar to the results estimated by Flower and Kennett (1994). Many existing studies have found a positive relation between temperature and atmospheric vapor capacity (Oard, 1990; Stephens, 1990; Haywood et al., 2000). For example, Oard (1990) established a relation between temperature and water vapor capacity. Theoretically, high precipitation requires the relatively rapid evaporation of seawater; as water evaporation is known to increase exponentially with temperature, such a rapid process will only occur over already warm water (Fig. 7A). Today's general precipitation trend as a function of latitude can be well explained by Oard's (1990) model: specifically, precipitation increases as temperatures rise (except in the subtropical high pressure belt between latitudes ~10°-30°) (Fig. 7B). Therefore, the warm and humid climatic conditions experienced by the eastern Longzhong Basin during the Mid-Miocene can be well explained by Oard's (1990) model, as well as by global precipitation patterns: during the global warming which characterized the MMCO, the higher water vapor capacity resulting from higher temperatures would have led to increased precipitation in the eastern Longzhong Basin, as also demonstrated by the abundant precipitation observed in lower latitudes (Fig. 7B). On the other hand, globally high temperatures could also result in sea level rises (Haq et al., 1987; Miller et al., 2005; Hansen et al., 2013). According to the estimates of Hansen et al. (2013), sea levels during the MMCO were up to ~75 m higher than at present. These high sea levels would not only have facilitated the transportation of precipitation to the study region (due to the relatively shorter distance between the water vapor source and its destination), but would also likely have resulted in a more balanced rainfall seasonality (similar to that of the Shanwang Basin, which is proximate to the sea to the east; Figs. 3, 7A). The reconstructed Miocene climatic parameters for the Wushan Basin and the Tianshui Basin also document a monsoonal climate similar to today's (Fig. 5A and B); this inference is supported by the paleosol records of the Yanwan Section in the Tianshui Basin (Pan et al., 2009) and the HZ-2 drilling core in the Linxia Basin (Wu et al., 2017) which neighbors the Wushan Basin and the Tianshui Basin to the west (Fig. 1B). Statistically-modeled experiments have shown that the uplift of the Tibetan Plateau has been, and continues to be, the most important trigger for any initiation and intensification of the Asian Monsoon (Manabe and Terpstra, 1974; Kutzbach et al., 1989; Raymo and Ruddiman, 1992; Liu and Yin, 2002). This being the case, the existence of a Miocene monsoonal climate similar to today's would suggest that the Tibetan Plateau experienced significant uplift during the

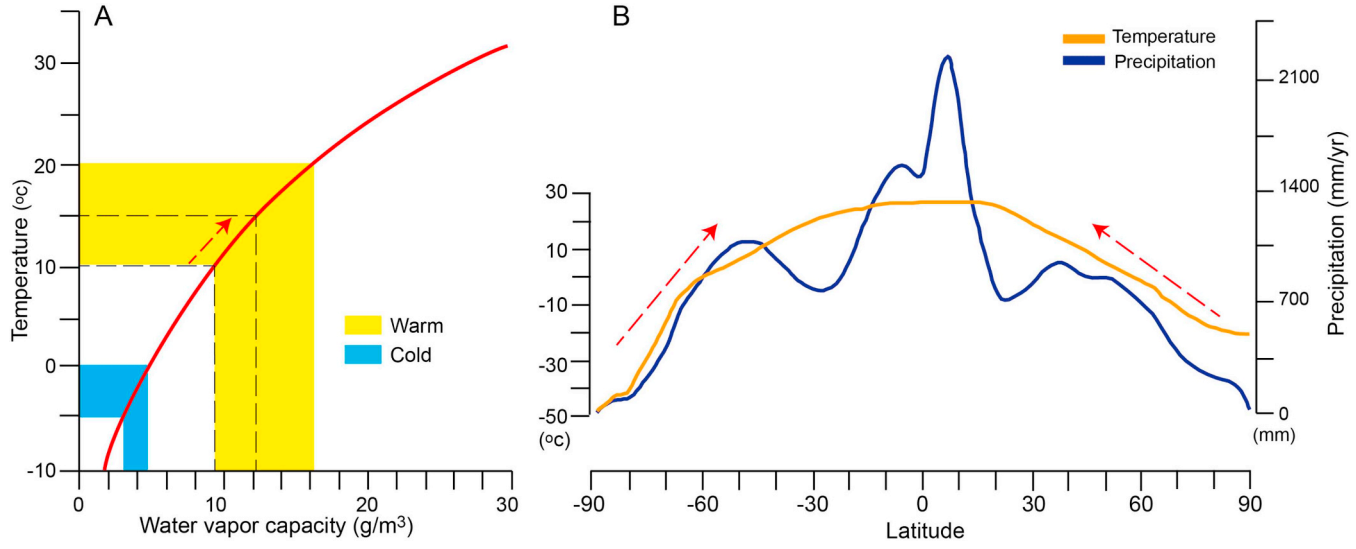

Fig. 7. (A) Water capacity at saturation (11% relative humidity (*RH*)) *versus* temperature (note the 14% raise in water capacity as the temperature increases from 10 to 15 °C). (B) Variations in MAT and MAP as a function of latitude for the present day (arrow showing the general relation between warming and an increase in precipitation). A and B are compiled from Miao et al. (2013, 2017).

Mid-Miocene, and that this period of uplift altered the general atmospheric circulation patterns over the Tibetan Plateau. According to Shi et al. (1999), this uplift event occurred during the ~25–17 Ma period. This event has been identified as the second phase of the Tibetan Plateau's uplift (or the second phase of the Himalayan movement), and resulted in the altitude of the Tibetan Plateau exceeding 2000 m above sea level (asl). Along with Mid-Miocene global warming, the expansion of the Asian continent and the shrinkage of the Paratethys Sea, and the expansion of the marginal seas of the western Pacific Ocean, this uplift stimulated and intensified the EASM. The strength of monsoonal winds is regulated by the thermal gradient that develops from the differential heating of land and sea (Webster et al., 1998). The temperature over the Tibetan Plateau is therefore be critical to the strength of the Asian Monsoon as it provides a heat source for the lower atmosphere during the summer, thus creating a vast low-pressure system over Central Asia which then draws in warm and humid air from the Pacific Ocean towards the Asian interior (Wu et al., 2012). Theoretically, the higher the altitude of the Tibetan Plateau, the greater the thermal gradient between the Pacific Ocean and the Asian continent (mainly due to the temperature lapse rate), and thus the greater the climatic seasonality of East Asia (Liu and Yin, 2002). The MMCO climatic parameters observed in the eastern Longzhong Basin would indicate the existence of more balanced climatic conditions (Table 3), which may in turn suggest either that the Tibetan Plateau had not attained its present altitude by that time, or that the Tibetan Plateau played a subordinate role in any climatic changes.

6. Conclusions

The two pollen flora assemblages from the Yanwan and Nanyu sections in the Tianshui Basin and Wushan Basin sub-basins of the eastern Longzhong Basin presented here indicate that the vegetation cover of these two sub-basins during the MMCO was composed of broadleaved deciduous forests and mixed coniferous and deciduous broadleaved forests, respectively, which grew under warm and humid climatic conditions. Climatic parameters for the period were obtained by applying the CoA to these two pollen flora databases. The values for the Tianshui Basin were: MAT 14.2–18.9 °C; WMT 22.5–26.6 °C; CMT 2.5–7.8 °C; MAP 797.5–1113.3 mm; MaMP 241–264 mm; MiMP 9–14.1 mm. The paleoclimatic parameters for the Wushan Basin are the same, or similar to, those of the Tianshui Basin, except for the MaMP value (*i.e.*, 141.5–268.1 mm). These climatic parameters would indicate the existence of much warmer and wetter climatic conditions, and a more seasonally-balanced climate. The higher temperatures and correspondingly higher precipitation values would favor the northwards shift in the growth of forest vegetation, potentially causing the humid region to expand northwestwards. The climatic conditions recorded by the climatic parameters obtained can be explained by the higher temperatures known to have occurred during the MMCO. This would suggest that global temperatures were a major driver of Mid-Miocene climate change in northern central China.

Supplementary data to this article can be found online at https://doi.org/10.1016/j.palaeo.2018.10.025.

Acknowledgments

This wok was co-supported by the National Natural Sciences Foundation of China (Grant Nos. 41877445, 41771209, 41671101 and 41301216), the State Program of the National Natural Sciences Foundation of China (Grant No. 41330745) and the Fundamental Research Funds for Central Universities (Grant No. lzujbky-2017-216). Special thanks to Editor Paul Hesse and two anonymous reviewers for their constructive suggestions and comments on this paper.

References

Alonso-Zarza, A.M., Zhao, Z., Song, C., Li, J., Zhang, J., Martín-Pérez, A., Martín-García, R., Wang, X., Zhang, Y., Zhang, M., 2009. Mudflat/distal fan and shallow lake sedimentation (upper Vallesian–Turolian) in the Tianshui Basin, Central China: evidence against the late Miocene eolian loess. Sediment. Geol. 222, 42–51.

Atlas of Physical Geography in China, 2000. China Cartographic Publishing House, Beijing, 2nd ed. (in Chinese).

Deng, T., 2016. Records and characteristics of the Mammalian faunas of Northern China in the middle Miocene Climatical Optimum. Quat. Sci. 36, 811–819 (in Chinese with English abstract).

Fagri, K., Iversen, J., 1989. Textbook of Pollen Analysis, 4th ed. John Wiley & Sons, New York, pp. 1–328.

Flower, B.P., Kennett, J.P., 1994. The middle Miocene climatic transition: East Antarctic ice sheet development, deep ocean circulation and global carbon cycling. Palaeogeogr. Palaeoclimatol. Palaeoecol. 108, 537–555.

Foster, G.L., Rohling, E.J., 2012. Relationship between sea level and climate forcing by CO_2 on geological timescales. In: Proceeding of the National Academy of Science of the United States of Americahttps://doi.org/10.1073/pnas.1216073110.

Goldner, A., Herold, N., Huber, M., 2014. The challenge of simulating the warmth of the mid-Miocene climatic optimum in CESM1. Clim. Past 10, 523–536.

Grimm, E.C., 1993. TILIA Version 2.0.b.4. Illinois State Museum, Springfield, Illinois, USA.

Hansen, J., Sato, M., Russell, G., Kharecha, P., 2013. Climate sensitivity, sea level and atmospheric carbon dioxide. Phil. Trans. R. Soc. A 371, 20120294 (20120210.20121098/rsta.20122012.20120294).

Haq, B.U., Hardenbot, J., Vail, P.R., 1987. Chronology of fluctuating sea levels since the Triassic. Science 235, 1156–1167.

Haywood, A.M., Valdes, P.J., Sellwood, B.W., 2000. Global scale palaeoclimate reconstruction of the middle Pliocene climate using the UKMO GCM: initial results. Glob. Planet. Chang. 25, 239–256.

He, K., 2013. Magnetostratigraphy and Paleoclimatic Significance of Miocene Sediment in Wushan Region. Master Thesis. Lanzhou Universitye, Lanzhou, pp. 1–60 (in Chinese with English Abstract).

Herold, N., Huber, M., Müller, R.D., 2011. Modelling the Miocene climatic optimum, part 1: land and atmosphere. J. Clim. 24, 6353–6372.

Herold, N., Huber, M., Müller, R.D., Seton1, M., 2012. Modeling the Miocene Climatic Optimum: Ocean Circulation. Paleoceanography 27PA1209. https://doi.org/10.1029/2010PA002041.

Hou, Z., Li, J., Song, C., Meng, J., Zhang, J., 2015. Late-Miocene palaeoecological evolution of the Tianshui Basin, NE Tibetan Plateau: evidence from stable organic carbon isotope record. J. Asian Earth Sci. 98, 296–303.

Hui, Z., Li, J., Song, C., Chang, J., Zhang, J., Liu, J., Liu, S., Peng, T., 2017. Vegetation and climatic changes during the Middle Miocene in the Wushan Basin, northeastern Tibetan Plateau: evidence from a high-resolution palynological record. J. Asian Earth Sci. 147, 116–127.

Hui, Z., Li, J., Xu, Q., Song, C., Zhang, J., Wu, F., Zhao, Z., 2011. Miocene vegetation and climatic changes reconstructed from a sporopollen record of the Tianshui Basin, NE Tibetan Plateau. Palaeogeogr. Palaeoclimatol. Palaeoecol. 308, 373–382.

IDBMC (Information Department of Beijing Meteorological Center), 2005. Land Climate Data of China (1971–2000) (Part II). China Meteorological Press, Beijing (in Chinese).

IPCC (Intergovernmental Panel on Climate Change), 2007. IPCC Fourth Assessment Report (AR4): Working Groups I, II, III and Synthesis Reports. http://www.ipcc.ch.

Kochhann, K.G.D., Holbourn, A., Kuhnt, W., Channell, J.E.T., Lyle, M., Shackford, J.K., Wilkens, R.H., Andersen6, N., 2016. Eccentricity pacing of eastern equatorial Pacific carbonate dissolution cycles during the Miocene Climatic Optimum. Paleoceanography 31, 1176–1192.

Kou, X.Y., Ferguson, D.K., Xu, J.X., Wamg, Y.F., Li, C.S., 2006. The reconstruction of paleovegetation and paleoclimate in the late pliocene of west Yunnan, China. Clim. Chang. 77, 431–448.

Kutzbach, J.E., Guetter, P.J., Ruddiman, W.F., Prell, W.L., 1989. Sensitivity of climate to Late Cenozoic uplift in southern Asia and the American west: numerical experiments. J. Geophys. Res. 94, 18393–18407.

Lease, R.O., 2014. Cenozoic mountain building on the northeastern Tibetan Plateau. In: Nie, J., Horton, B.K., Hoke, G.D. (Eds.), Toward an Improved Understanding of Uplift Mechanisms and the Elevation History of the Tibetan Plateau: Geological Society of America Special Paper. 507. pp. 115–127. https://doi.org/10.1130/2014.2507(1106).

Lebreton-Anberree, J., Li, S., Li, S.F., Spicer, R.A., Zhang, S.T., Su, T., Deng, C., Zhou, Z.K., 2016. Lake geochemistry reveals marked environmental change in Southwest China during the Mid Miocene Climatic Optimum. Sci. Bull. https://doi.org/10.1007/s11434-016-1095-x.

Li, J., Feng, Z., Tang, L., 1988. Late Quaternary monsoon patterns on the loess plateau of China. Earth Surf. Process. Landf. 13, 125–135.

Li, J., Zhang, J., Song, C., Zhao, Z., Zhang, Y., Wang, X., Zhang, J., Cui, Q., 2006. Miocene Bahean stratigraphy in the Longzhong Basin, northern central China and its implications in environmental change. Sci. China Earth Sci. 49, 1270–1279.

Liang, M.M., Bruch, A., Collinson, M., Mosbrugger, V., Li, C.S., Sun, Q.G., Hilton, J., 2003. Testing the climatic estimates from different palaeobotanical methods: an example from the Middle Miocene Shanwang flora of China. Palaeogeogr. Palaeoclimatol. Palaeoecol. 198, 279–301.

Liu, J., Li, J.J., Song, C.H., Yu, H., Peng, T.J., Hui, Z.C., Ye, X.Y., 2016. Palynological evidence for late Miocene stepwise aridification on the northeastern Tibetan Plateau. Clim. Past 12, 1473–1484.

Liu, S., Li, J., Stockli, D.F., Song, C., Nie, J., Peng, T., Wang, X., He, K., Hui, Z., Zhang, J., 2015. Late Tertiary reorganizations of deformation in northeastern Tibet constrained by stratigraphy and provenance data from eastern Longzhong Basin. J. Geophys. Res. Solid Earth 120, 5804–5821. https://doi.org/10.1002/2015JB011949.
Liu, X., Yin, Z., 2002. Sensitivity of East Asian monsoon climate to the uplift of the Tibetan Plateau. Palaeogeogr. Palaeoclimatol. Palaeoecol. 183, 223–245.
Manabe, S., Terpstra, T.B., 1974. The effects of mountains on the general circulation of the atmosphere as identified by numerical experiments. J. Atmos. Sci. 31, 3–42.
Miao, Y., Herrmann, M., Wu, F., Yan, X., Yang, S., 2012. What controlled Mid–Late Miocene long-term aridification in Central Asia? — Global cooling or Tibetan Plateau uplift: a review. Earth Sci. Rev. 112, 155–172.
Miao, Y., Song, C., Fang, X., Meng, Q., Zhang, P., Wu, F., Yan, X., 2016. Late Cenozoic genus *Fupingopollenites* development and its implications for the Asian summer monsoon evolution. Gondwana Res. 29, 320–333.
Miao, Y., Warny, S., Clift, P.D., Liu, C., Gregory, M., 2017. Evidence of continuous Asian summer monsoon weakening as a response to global cooling over the last 8 Ma. Gondwana Res. 52, 48–58.
Miao, Y.F., Fang, X.M., Herrmann, M., Wu, F.L., Zhang, Y.Z., Liu, D.L., 2011. Miocene pollen record of KC–1 core in the Qaidam Basin, NE Tibetan Plateau and implications for evolution of the East Asian monsoon. Palaeogeogr. Palaeoclimatol. Palaeoecol. 299, 30–38.
Miao, Y.F., Fang, X.M., Wu, L.F., Cai, M.T., Song, C.H., Meng, Q.Q., Xu, L., 2013. Late Cenozoic continuous aridification in the western Qaidam Basin: evidence from sporopollen records. Clim. Past 9, 1863–1877.
Miller, K.G., Kominz, M.A., Browning, J.V., Wright, J.D., Mountain, G.S., Katz, M.E., Sugarman, P.J., Cramer, B.S., Christie-Blick, N., Pekar, S.F., 2005. The Phanerozoic record of global sea-level change. Science 310, 1293–1298.
Mosbrugger, V., Utescher, T., 1997. The coexistence approach - a method for quantitative reconstructions of Tertiary terrestrial palaeoclimate data using plant fossils. Palaeogeogr. Palaeoclimatol. Palaeoecol. 134, 61–86.
Oard, M.J., 1990. An Ice Age Caused by the Genesis Flood. Institute for Creation Research, El Cajon, California, pp. 5.
Pan, M., Song, C., Li, J., Zhang, J., Zhang, P., Hui, Z., 2009. Micromorphological characteristics of Miocene palaeosol and their paleoenvironment significances in Tianshui, Gansu. Acta Pedol. Sin. 46, 578–585 (in Chinese with English abstract).
Peng, T., Li, J., Song, C., Guo, B., Liu, J., Zhao, Z., Zhang, J., 2016. An integrated biomarker perspective on Neogene Quaternary climatic evolution in NE Tibetan Plateau: Implications for the Asian aridification. Quat. Int. 399, 174–182.
Peng, T., Li, J., Song, C., Zhao, Z., Zhang, J., Hui, Z., King, J.W., 2012. Biomarkers challenge early Miocene loess and inferred Asian desertification. Geophys. Res. Lett. 39, L06702 (doi:06710.01029/02012GL050934).
Quan, C., Liu, Y.-S.C., Utescher, T., 2012. Eocene monsoon prevalence over China: a paleobotanical perspective. Palaeogeogr. Palaeoclimatol. Palaeoecol. 365-366, 302–311.
Raymo, M.E., Ruddiman, W.F., 1992. Tectonic foring of late Cenozoic climate. Nature 359, 117–122.
Scotese, C.R., 2002. PALEOMAP Website. http://www.scotese.com.
Shackleton, N.J., Kennett, J.P., 1975. Paleotemperature history of the Cenozoic and the initiation of Antarctic glaciation: oxygen and carbon isotope analyses in DSDP Sites 277, 279 and 281. Initial Rep. Deep Sea Drill. Proj. 29, 743–755.
Shi, Y., Tang, M., Ma, Y., 1999. Linkage between the second uplifting of the Qinghai-Xizang (Tibetan) Plateau and the initiation of the Asian monsoon system. Sci. China Ser. D Earth Sci. 42, 303–312.
Song, Y., Wang, Q., An, Z., Qiang, X., Dong, J., Chang, H., Zhang, M., Guo, X., 2017. Mid-Miocene climatic optimum: Clay mineral evidence From the red clay succession, Longzhong Basin, Northern China. Palaeogeogr. Palaeoclimatol. Palaeoecol. https://doi.org/10.1016/j.palaeo.2017.1010.1001.
Song, Z., 1999. Fossil Spores and Pollen of China. vol. 1 Science Press, Beijing (in Chinese).
Stephens, G.L., 1990. On the relationship between water vapor over the oceans and sea surface temperature. J. Clim. 3 (6), 634–645.
Sun, Q.G., Collinson, M.E., Li, C.S., Wang, Y.F., Beerling, D.J., 2002. Quantitative reconstruction of palaeoclimate from the Middle Miocene Shanwang flora, eastern China. Palaeogeogr. Palaeoclimatol. Palaeoecol. 180, 315–329.
Tong, J.A., Youa, Y., Müller, R.D., Seton, M., 2009. Climate model sensitivity to atmospheric CO_2 concentrations for the middle Miocene. Glob. Planet. Chang. 67, 129–140.
Utescher, T., Bruch, A.A., Erdei, B., François, L., Ivanov, D., Jacques, F.M.B., Kern, A.K., Liu, Y.-S.C., Mosbrugger, V., Spicer, R.A., 2014. The Coexistence Approach–theoretical background and practical considerations of using plant fossils for climate quantification. Palaeogeogr. Palaeoclimatol. Palaeoecol. 410, 58–73.
Wan, S., Kurschner, W.M., Clift, P.D., Li, A., Li, T., 2009. Extreme weathering/erosion during the Miocene Climatic Optimum: evidence from sediment record in the South China Sea. Geophys. Res. Lett. 36, L19706 (doi:19710.11029/12009GL040279).
Wang, F., Qian, N., Zhang, Y., Yang, H., 1995. Pollen Flora of China, 2nd ed. Science Press, Beijing, pp. 1–461 (in Chinese).
Wang, P.X., 1999. Response of Western Pacific marginal seas to glacial cycles: paleoceanographic and sedimentological features. Mar. Geol. 156, 5–39.
Wang, X., Deng, L., Zattin, M., Ji, M., Li, J., 2017. Palaeogene growth of the northeastern Tibetan Plateau: Detrital fission track and sedimentary analysis of the Lanzhou basin, NW China. J. Asian Earth Sci. 147, 322–331.
Wang, X., Song, C., Zattin, M., He, P., Song, A., Li, J., Wang, Q., 2016. Cenozoic pulsed deformation history of northeastern Tibetan Plateau reconstructed from fission-track thermochronology. Tectonophysics 672-673, 212–227.
Wang, Z., Zhang, P., Carmala, N.G., Richard, O.L., Zhang, G., Zheng, D., Brian, H., Yuan, D., Li, C., Liu, J., Wu, Q., 2012. Magnetostratigraphy and depositional history of the Miocene Wushan basin on the NE Tibetan plateau, China: Implications for middle Miocene tectonics of the West Qinling fault zone. J. Asian Earth Sci. 44, 189–202.
Webster, P.J., Magana, V.O., Palmer, T.N., Shukla, J., Tomas, R.A., Yanai, M., Yasunari, T., 1998. Monsoons: processes, predictability, and the prospects for prediction, in the TOGA decade. J. Geophys. Res. 103, 14451–14510.
Wu, F., Fang, X., Meng, Q., Zhao, Y., Tang, F., Zhang, T., Zhang, W., Zan, J., 2017. Magneto- and litho-stratigraphic records of the Oligocene-Early Miocene climatic changes from deep drilling in the Linxia Basin, Northeast Tibetan Plateau. Glob. Planet. Chang. 158, 36–46.
Wu, G., Liu, Y., He, B., Bao, Q., Duan, A., Jin, F.F., 2012. Thermal controls on the Asian summer monsoon. Sci. Rep. 2, 404 (doi: 410.1038/srep00404).
Wu, Z.Y., Wang, X.F., Liu, F.Y., Zhu, Y.C., Li, S.Y., Li, B., He, S.Y., Zhang, X.S., Chen, C.D., Zhou, Y.L., Zhou, G.Y., Lin, Y., Hou, X.Y., 1980. Vegetation of China. Science Press, Beijing (in Chinese).
Xu, Q., Li, Y., Li, Y., Yang, X., Zhang, Z., Jia, H., 2006. A dicussion about modern pollen process and study Quaternary environment. Prog. Nat. Sci. 16, 647–656 (in Chinese).
Yang, J., Wang, Y.F., Spicer, R.A., Mosbrugger, V., Li, C.S., Sun, Q.G., 2007. Climatic reconstruction at the Miocene Shanwang Basin, China, using leaf margin analysis, clamp, coexistence approach, and overlapping distribution analysis. Am. J. Bot. 94, 599–608.
You, Y., 2010. Climate-model evaluation of the contribution of sea-surface temperature and carbon dioxide to the Middle Miocene Climate Optimum as a possible analogue of future climate change. Aust. J. Earth Sci. 57, 207–219.
You, Y., Huber, M., Muller, R.D., Poulsen, C.J., Ribbe, J., 2009. Simulation of the Middle Miocene Climate Optimum. Geophys. Res. Lett. 36, L04702. https://doi.org/10.1029/2008GL036571.
Zachos, J., Pagani, M., Sloan, L., Thomas, E., Billups, K., 2001. Trends, rhythms, and aberrations in global climate 65 Ma to present. Science 292, 686–693.
Zan, J., Fang, X., Yan, M., Zhang, W., Lu, Y., 2015. Lithologic and rock magnetic evidence for the Mid-Miocene Climatic Optimum recorded in the sedimentary archive of the Xining Basin, NE Tibetan Plateau. Palaeogeogr. Palaeoclimatol. Palaeoecol. 431, 6–14.
Zhai, Y., Cai, T., 1984. The Tertiary system of Gansu province. In: Gansu Geology. People's Press of Gansu, Lanzhou, China, pp. 1–40 (in Chinese).
Zhang, J., Li, J., Song, C., Zhao, Z., Xie, G., Wang, X., Hui, Z., Peng, T., 2013. Paleomagnetic ages of Miocene fluvio-lacustrine sediments in the Tianshui Basin, western China. J. Asian Earth Sci. 62, 341–348.
Zhao, H., Sun, Y., Qiang, X., 2017. Iron oxide characteristics of mid-Miocene Red Clay deposits on the western Chinese Loess Plateau and their paleoclimatic implications. Palaeogeogr. Palaeoclimatol. Palaeoecol. 468, 162–172.